

Inverse transitions and disappearance of the λ -line in the asymmetric random-field Ising and Blume-Capel models

Santanu Das^{*} and Sumedha[†]

*School of Physical Sciences, National Institute of Science Education and Research, Jatni 752050, India
and Homi Bhabha National Institute, Training School Complex, Anushakti Nagar 400094, India*

 (Received 17 March 2023; revised 13 July 2023; accepted 6 October 2023; published 24 October 2023)

We report on reentrance in the random-field Ising and Blume-Capel models, induced by an asymmetric bimodal random-field distribution. The conventional continuous line of transitions between the paramagnetic and ferromagnetic phases, the λ -line, is wiped away by the asymmetry. The phase diagram, then, consists of only first-order transition lines that always end at ordered critical points. We find that, while for symmetric random-field distributions there is no reentrance, the asymmetry in the random-field results in a range of temperatures for which magnetization shows reentrance. While this does not give rise to an inverse transition in the Ising model, for the Blume-Capel model, however, there is a line of first-order inverse phase transitions that ends at an inverse-ordered critical point. We show that the location of the inverse transitions can be inferred from the ground-state phase diagram of the model.

DOI: [10.1103/PhysRevE.108.L042101](https://doi.org/10.1103/PhysRevE.108.L042101)

Introduction. Inverse transitions are an unusual class of phase transitions where the ordered phase has more entropy than the disordered phase and hence occurs at a higher temperature [1]. This entropy-driven phase reentrance of the ordered phase is widely observed [2]. Examples include ferroelectric thin films [3]; perpendicularly magnetized ultrathin ferromagnetic films [4–6]; anisotropic dipolar magnets [7]; polymer systems such as poly(4-methyl-1-pentene) [8,9]; the solutions of cyclodextrin, water, and methylpyridine [10,11]; inverse melting between lattice and disordered vortex phase in high-temperature superconductors [12]; and shear thickening in glasses and granular systems [13].

Models with spin-1 variables like the Ghatak-Sherrington model have been found to exhibit inverse transition (IT) in some recent studies [13–26]. These studies have focused on models with a glassy phase and random bond interactions, where it is expected that frustration and disorder allow for a possibility of inverse freezing (a glass to liquid transition on cooling). Reentrance is also seen in dipolar long- and short-range models with asymmetric random interaction and Gaussian random fields [27]. However, in general, it is expected that random fields will suppress the IT [22].

In this work, we study the random-field Ising model (RFIM) and the random-field Blume-Capel model (RFBCM) with ferromagnetic interactions and an asymmetric bimodal distribution (BD) for the random field. These models do not have a glass phase. Also, the models with the symmetric BD for the quenched random fields have no ITs [28,29]. Any asymmetry in the random-field distribution is expected to make the system less random and, hence, no ITs are expected. In this paper, we undertake an expansive study of

the infinite-range RFIM and RFBCM with asymmetric BDs and report a number of interesting results. Infinite-range interaction models usually belong to the same universality class as the mean-field models with fixed coordination numbers. Generically, we find that even an infinitesimal asymmetry changes the phase diagram nontrivially. Interestingly, there is a line of inverse first-order transitions in the phase diagram of the asymmetric RFBCM. While there have been some studies of these models with symmetric distributions [28–31], asymmetric distributions have hitherto been studied for the RFIM [32–34]. Disorder distribution is typically asymmetric in real experiments [32]. We find that an asymmetric RFBCM shows first-order ITs similar to those seen in experiments that display inverse melting [8–11].

For symmetric BD, the RFIM has a line of continuous transitions (the λ -line) that meets a line of first-order transitions at a tricritical point (TCP) [35]. We find that even a slight asymmetry wipes away the λ -line and the TCP in the RFIM. We instead find a phase diagram consisting of a line of first-order transitions that ends at a critical point. The magnetization (m) is nonzero at this point and, hence, we call this an ordered critical point (OCP) [36]. The location of the OCP to a good approximation is determined by the location of the first-order transition in the ground-state phase diagram of the model. Hence, even at finite temperature (T) the phase diagram is dominated by the random-field disorder.

The fluid separation in porous media is considered a good realization of the RFIM [37–39]. The results from experiments on these models found the value of the order-parameter exponent to be closer to the value for the pure Ising model rather than to that for the RFIM with symmetric random-field distribution [37]. It was suggested that these experiments should be compared with the asymmetric RFIM [32]. In more recent experiments it is shown that they exhibit out-of-equilibrium disorder-driven behavior similar to that of the

*santanudas@niser.ac.in

†sumedha@niser.ac.in

athermal nonequilibrium RFIM [39,40]. Consistent with the experiments, we find that the value of the exponent near an OCP is the same as the pure Ising critical point.

Another interesting observation is the nonmonotonic behavior of m as a function of T for both an asymmetric RFIM and an asymmetric RFBCM. We find that for the values of the parameters close to an OCP, m can become nonmonotonic. Though in the absence of the crystal field (Δ), there is no IT in these models. We show that, for the RFBCM for a range of Δ , m jumps to a higher value on increasing T . The system has a first-order IT which we show is entropy driven. The magnitude of the jump decreases with increasing T and the line of the first-order IT ends at an inverse OCP. We hence report a mechanism for ITs which crucially depends on the asymmetry of the disorder distribution. This is an inverse melting transition since the system goes from a less-ordered state to a more-ordered state on increasing T . We also find that the RFBCM has two first-order transitions with increasing T for a narrow range of parameters: first from a less-ordered state to a more-ordered state and then again to a less-ordered state, similar to the two first-order transitions observed in recent experiments involving solutions of cyclodextrin, water, and methylpyridine [11]. The RFBCM also shows a reentrance in the quadrupole moment (q) for some range of the parameters. We show that the ground-state phase diagram crucially determines the phase diagram at finite T .

Model. The Hamiltonian for the infinite-range RFIM and RFBCM can be written as

$$\mathcal{H} = -\frac{1}{2N} \left(\sum_{i=1}^N s_i \right)^2 + \Delta \sum_{i=1}^N s_i^2 - \sum_{i=1}^N h_i s_i, \quad (1)$$

where $s_i = \pm 1$ and $s_i = 0, \pm 1$ for the RFIM and the RFBCM, respectively. The crystal field is represented by Δ . It is 0 for the RFIM. The RFBCM with $s_i = 0$ and ± 1 and $\Delta = 0$ has a behavior which is similar to that of the RFIM with $s_i = \pm 1$. We hence call it the RFIM with $s = 1$.

The magnetic field h_i associated with each site is an independent and identically distributed random variable taken from the BD of the form

$$Q(h_i) = r\delta(h_i - h_0) + (1-r)\delta(h_i + h_0), \quad (2)$$

with bias r and strength h_0 . The above distribution is asymmetric when $r \neq 1/2$. We take $h_0 > 0$ and consider $r \in [1/2, 1]$.

The probability of a spin configuration C_N with the magnetization $x_1 = \sum_i s_i/N$ and the quadrupole moment $x_2 = \sum_i s_i^2/N$ satisfies the large deviation principle, i.e., $P(C_N : x_1, x_2) \sim e^{-NI(x_1, x_2)}$. I is the rate function that can be calculated using large deviations. The free energy of the system is then the infimum of I with respect to x_1 and x_2 . It is, hence, enough to consider only the fixed points of I to write the generalized free energy functional of the model. We hence obtain an expression for the free energy functional of the model with quenched random fields (see Ref. [30] for details) as

$$\tilde{f}(x_1) = \frac{1}{2}\beta x_1^2 - \langle \log[c + 2e^{-\beta\Delta} \cosh \beta(x_1 + h_i)] \rangle_{\{h_i\}}, \quad (3)$$

where $\beta = 1/T$, $c = 0$ for the RFIM and $c = 1$ for the RFBCM. The value of x_1 that minimizes $\tilde{f}(x_1)$ is the magneti-

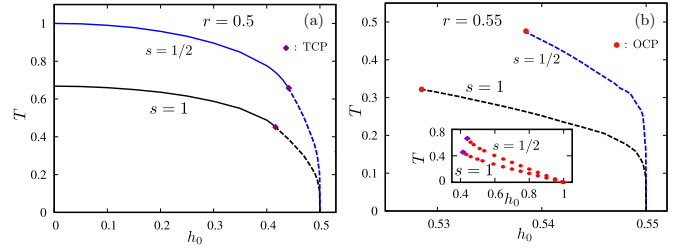


FIG. 1. Phase diagram in the $(T-h_0)$ plane for the RFIM ($s = \pm 1$) (blue) and its spin-1 variant ($s = 0, \pm 1$) (black) for (a) the symmetric BD ($r = 0.5$) and (b) the asymmetric BD ($r = 0.55$). Solid lines are the lines of continuous transitions and the dashed lines are the lines of first-order transitions. A rhombus (purple) represents the TCP and a circle (red) represents an OCP. The inset of panel (b) plots the locus of the TCP (rhombus) and the OCP (circle) in the $(T-h_0)$ plane for $1/2 \leq r \leq 1$. With increasing r , the OCP occurs at a lower value of T and higher value of h_0 .

zation m and the quadrupole moment $q = \frac{1}{\beta} \partial \tilde{f}(x_1) / \partial \Delta|_{x_1=m}$. These are given by

$$m = \left\langle \frac{2e^{-\beta\Delta} \sinh \beta(m + h_i)}{c + 2e^{-\beta\Delta} \cosh \beta(m + h_i)} \right\rangle_{\{h_i\}} \quad (4)$$

and the quadrupole moment

$$q = \left\langle \frac{2e^{-\beta\Delta} \cosh \beta(m + h_i)}{c + 2e^{-\beta\Delta} \cosh \beta(m + h_i)} \right\rangle_{\{h_i\}}. \quad (5)$$

Here $\langle \rangle_{\{h_i\}}$ represents the average over random-field distribution.

RFIM for $s = 1/2$ and $s = 1$. The phase diagram of the RFIM for the symmetric BD has long been known [35,41]. It has a line of continuous transitions between ordered and disordered phases for the weak disorder strength (low h_0) that ends at a TCP. On further increasing h_0 , there is a line of first-order transitions that ends at $h_0 = 1/2$ and $T = 0$. The qualitative phase behavior remains unchanged for the spin-1 system in the absence of Δ [see Fig. 1(a)].

Interestingly, we find that for an asymmetric BD [Eq. (2)], asymmetry in the distribution wipes out the line of continuous transitions along with the TCP. The phase diagram only has a line of first-order transitions that starts at $h_0 = r$ and $T = 0$ and ends at an OCP. As r deviates from $1/2$ and approaches 1, the OCP occurs at a lower value of T and approaches 0 as $r \rightarrow 1$ [see Fig. 1(b)]. Since m is finite at an OCP, to find the coordinates of the OCP we equate the first three derivatives of $\tilde{f}(x_1)$ to 0. The meeting point of the solution of the three equations, for a given r , Δ , and h_0 , gives the coordinates of the OCP [42]. In Fig. 2 for $s = 1/2$ we have plotted the magnetization and the susceptibility at three different points in the phase diagram: at the OCP, at a point on the line of first-order transitions between $m \approx 1$ and $m \approx 2r - 1$, and for a point near the first-order line where there is no transition but magnetization m is nonmonotonic. Similar behavior occurs for $s = 1$ as well. We find that for both $s = 1/2$ and $s = 1$, m shows a nonmonotonic dependence on T for any $r > 1/2$ and $h_0 > r$. The degree of nonmonotonicity is maximum when r is close to $1/2$ and h_0 is just above r .

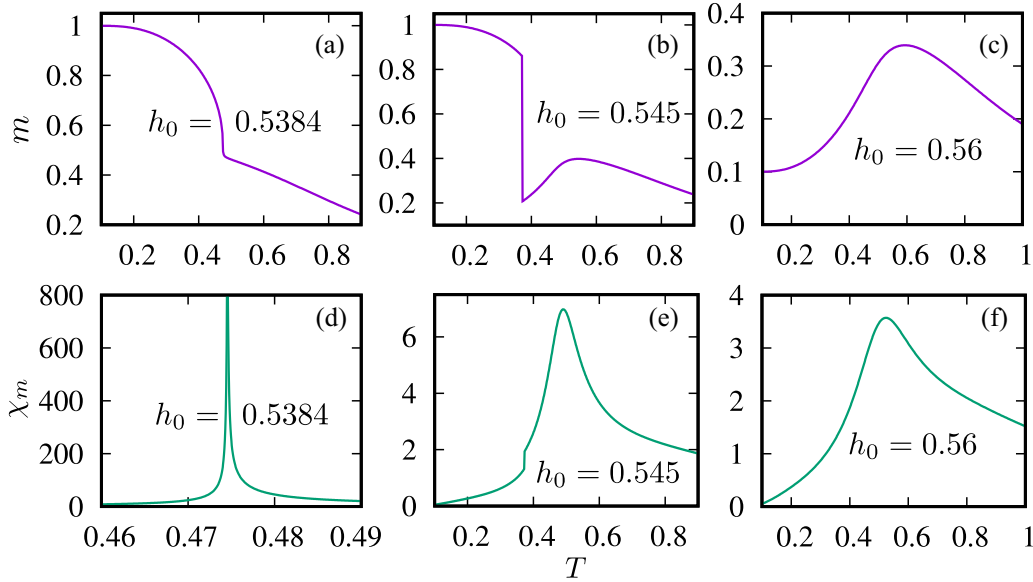


FIG. 2. Magnetization (m) and magnetic susceptibility (χ_m) for the RFIM with $s = 1/2$ and $r = 0.55$ are plotted at the OCP [panels (a) and (d)], at a point along the first transition line [panels (b) and (e)] and for h_0 near the first-order transition line with reentrance in m [panels (c) and (f)].

We find that the OCP lies in the critical Ising universality class and m scales with the exponent $\beta = 1/2$ near an OCP as T increases. On the other hand, $\beta = 1/4$ for a TCP. This is verified in Fig. 3, where we contrast the scaling of magnetization near a TCP and an OCP by taking the symmetric BD and the asymmetric BD, respectively.

The RFBCM and the reentrance transition. For spin-1, on the introduction of the Δ , i.e., for the RFBCM we find that there is a first-order reentrance transition for the asymmetric BD for a range of Δ values. The transition becomes a continuous reentrance transition at (Δ_c, T_c) that depends on the values of r and h_0 [see Fig. 4(a)]. We also find that depending on the value of r , there is also a possibility of a second first-order transition from a more-ordered to a less-ordered state in the model [see Fig. 4(b)].

To understand the phase behavior at finite temperature, we first study the ground state ($T = 0$). In the ground state, the disorder averaged energy is given by $\min_m \phi(m)$, where $\phi(m) = \lim_{\beta \rightarrow \infty} \beta^{-1} \tilde{f}(m)$. We find that the ground-state ($T = 0$) phase diagram of the RFBCM has four phases (three

ferromagnetic phases, $F1$, $F2$, and $F3$, and one nonmagnetic phase, NM). These phases are separated by the lines of first-order transitions (see Fig. 5). These transitions can be understood by looking at the configurational entropy of these states. For example, the phases $F2$ and $F3$ have the same configurational entropy because in both phases spins take two values: in $F3$, ± 1 , and in $F2$, 0 and 1. As Δ increases, 0 spins become more favorable energetically and first there is a transition from $F3$ to $F2$ and finally to NM (phase with all spins 0). As T increases, each point on these first-order transition lines changes its position and ends at an OCP. The phase diagram of the model in the $(T-h_0)$ plane, for different ranges of Δ for $r = 0.55$, is shown in Fig. 6. We find that the finite T phase diagrams only have lines of first-order transitions and OCPs. This is very different from the phase diagrams for the RFBCM with symmetric bimodal and trimodal distributions [28–30]. For symmetric distributions, the phase diagrams consist of lines of first- and second-order transitions and various multicritical points.

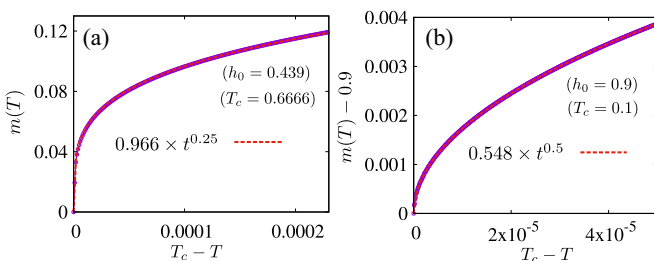


FIG. 3. Magnetization ($m \sim t^\beta$) versus the scaled temperature $t = T_c - T$ for the RFIM is plotted in the vicinity of the TCP and the OCP in panels (a) and (b) for $r = 0.5$ and 0.9 , respectively. The points are the numerical value of the magnetization m and the red dashed line is the scaling fit in both the cases.

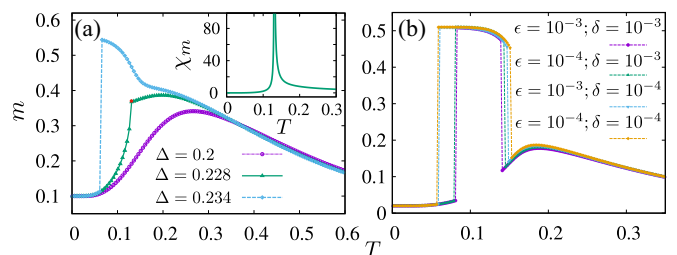


FIG. 4. (a) m versus T for the RFBCM for $r = 0.55$ and $h_0 = 0.56$ for different Δ values. The red dot is the OCP. In the inset, the susceptibility for the critical $\Delta = 0.228$ (OCP) is plotted. (b) m versus T for the RFBCM for $r = 0.51$ with small ϵ and δ where $h_0 = r + \epsilon$ and $\Delta = h_0 - (3r - 1)/2 - \delta$.

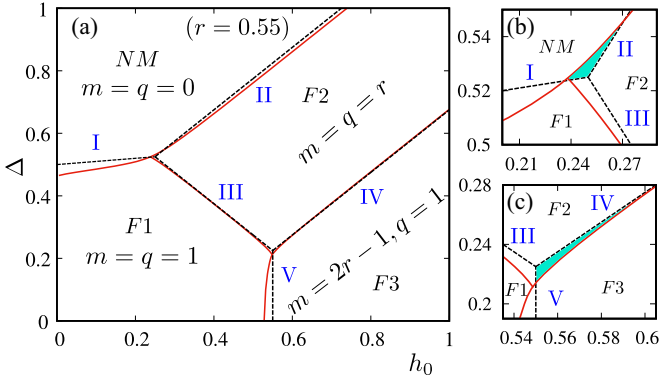


FIG. 5. (a) The $T = 0$ phase diagram in the $(\Delta-h_0)$ plane for $r = 0.55$ with three ferromagnetic phases, $F1$, $F2$, and $F3$, and a non-magnetic phase, NM . Black dashed lines are the lines of first-order transitions between the two neighboring phases at $T = 0$ given by I: $\Delta = 1/2 - (1 - 2r)h_0$, II: $\Delta = h_0 + r/2$, III: $\Delta = (1 + r)/2 - h_0$, IV: $\Delta = h_0 - (3r - 1)/2$, and V: $h_0 = r$. Solid red lines are the projection of the OCPs in the $(\Delta-h_0)$ plane. In panels (b) and (c) we enlarge the vicinity of the two triple points. The shaded part shows the range of parameters for which the IT in m occurs.

Depending on the strength of the crystal field, there are six different finite-temperature phase diagrams for the asymmetric BD. The phase diagram for the asymmetric BD for $r = 0.55$ in the $(T-h_0)$ plane for $\Delta < \Delta_1 (= 0.211)$ is similar to the $\Delta = 0$ case: a single first-order line of transitions separates $m \approx 1$ from $m \approx 2r - 1$ and ends at an OCP [see Fig. 6(a)]. For $\Delta > \Delta_1$, interestingly we find two lines of first-

order transitions, both ending at OCPs. For $\Delta_1 < \Delta < \Delta_2 (= 0.296)$, one of them corresponds to the usual first-order transition from a more-ordered to a less-ordered state (shown in black) and the other is a line of first-order ITs (shown in blue) between states with $m \approx 2r - 1$ and $m \approx r$ [see Figs. 6(b) and 6(c)]. On further increasing Δ , the reentrance transition in m changes to a reentrance transition in q as shown by the green lines in Figs. 6(d), 6(e), and 6(f). For $0.525 < \Delta < 0.545$, near the second triple point in the ground state [Fig. 5(b)], the IT occurs for both m and q as shown in Fig. 6(e).

We projected the OCPs onto the ground-state phase diagram of the model and identified the region in the $(\Delta-h_0)$ plane where the IT occurs. Corresponding to the first-order line of transitions in the ground-state phase diagram, we find a line of projection of OCPs in the $(\Delta-h_0)$ plane [Fig. 5(a)]. When this line of projections of OCPs enters into either the $F3$ or the NM phase, there is a region in the $(\Delta-h_0)$ plane where the reentrance transition takes place. For $r = 1/2$ this region shrinks to zero and there is no reentrance. In Figs. 5(b) and 5(c) the range of (Δ, h_0) for which there is an IT in m is shown shaded for $r = 0.55$. The reentrance region at first increases with r and then shrinks as $r \rightarrow 1$.

To find the region in the phase diagram where reentrance occurs, we fixed $h_0 \gtrsim r$ and gradually increased Δ . For example, for $r = 0.55$ and $h_0 = 0.56$, we find first-order reentrance transition for $0.228 \leq \Delta \leq 0.235$ [Fig. 4(a)]. As $\Delta \rightarrow 0.228$ there is still a reentrance, but without a jump in m . We find that this point is, in fact, an OCP. The inset of Fig. 4(a) shows the divergence of the magnetic susceptibility at the OCP.

We also find that if we take Δ and h_0 very close to the triple point of the $T = 0$ phase diagram for $r \gtrsim 1/2$, then there are two first-order transitions with the increase of T [see the inset of Fig. 6(b)]. For example, for $r = 0.51$, when we set $h_0 = r + \epsilon$ and $\Delta = h_0 - (3r - 1)/2 - \delta$ (where ϵ and δ are small) in the vicinity of the triple point, we observe two first-order transitions. For $r = 0.51$ this is shown in Fig. 4(b). This double first-order transition is similar to the one seen in experiments with solutions of cyclodextrin, water, and 4-methylpyridine which go from low-density liquid to high-density liquid to low-density liquid on increasing T via two first-order transitions [11].

If instead of fixing h_0 , we fix $\Delta \gtrsim (1 + 2r)/4$, then also we find a region in the phase diagram where the reentrance transition occurs. In fact, the phase diagrams in the $(T-\Delta)$ plane are similar to the phase diagrams in the $(T-h_0)$ plane.

Concluding remarks. We showed that the asymmetry in the random-field distribution results in a nonmonotonic behavior of the order parameter in the ferromagnetic models with quenched random fields that becomes an IT upon the introduction of Δ . To understand this let us look at the $T = 0$ phase diagram again. At $T = 0$, there is a residual m of order $2r - 1$ at low Δ and high h_0 for asymmetric BD (phase $F3$ in Fig. 5). For symmetric BD the $F3$ becomes a paramagnetic phase, and if Δ and h_0 are chosen such that the system is in this state at $T = 0$, then the system continues to stay in that state with $m = 0$ on increasing T as $m = 0$ maximizes entropy. On the other hand for $r \gtrsim 1/2$ and for Δ and h_0 very close to the triple point in Fig. 5(c), m increases as T increases and then jumps to r at the IT transition point. The

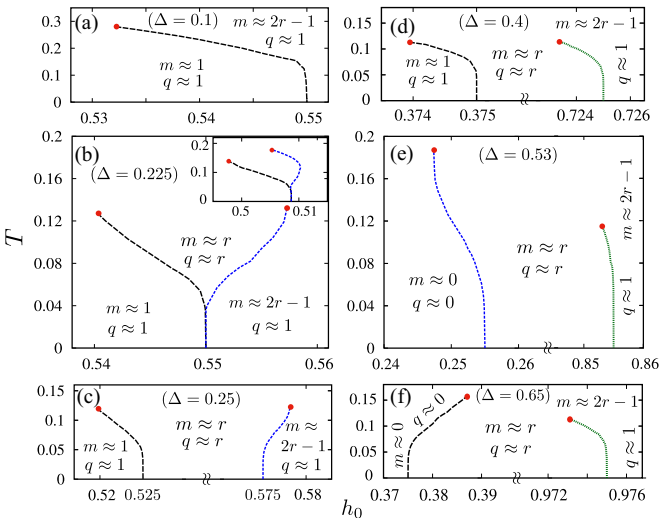


FIG. 6. Different phase diagrams for the RFBCM for different ranges of Δ in the $(T-h_0)$ plane for $r = 0.55$. (a) $-\infty < \Delta \leq 0.211$, (b) $0.211 < \Delta \leq 0.225$, (c) $0.225 < \Delta \leq 0.296$, (d) $0.296 < \Delta \leq 0.524$, (e) $0.524 < \Delta < 0.545$, and (f) $\Delta > 0.545$. Black lines are the lines of usual first-order transition, blue lines are the lines of first-order IT in m , and green lines are the lines of first-order IT in q . Red dots are the OCPs. The inset in panel (b) shows the phase diagram for $r = 0.51$, where the first-order transition line (blue) bends back, giving rise to two first-order transitions as a function of T for fixed h_0 .

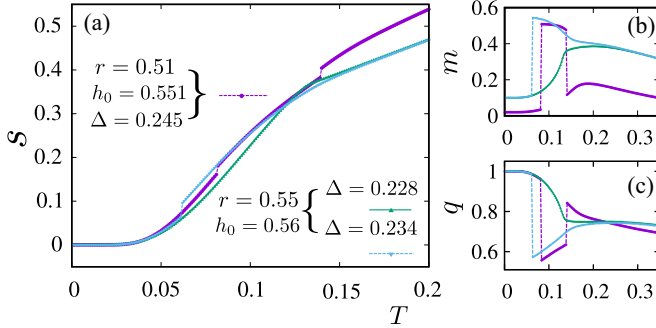


FIG. 7. Plots of entropy s , m , and q as a function of T for OCPs (solid green line), near the IT when there is only one first-order transition (dashed blue line) and for the case where there are two first-order transitions (dashed purple line).

entropy (s) also jumps at that point (Fig. 7). Since an infinitesimal amount of asymmetry can give rise to IT, it is possible that the topology of finitely connected graphs with heterogeneous degree distribution can induce that asymmetry and give rise to the topology-induced IT as seen in some studies [43,44].

The value of Δ and h_0 at which the IT occurs is close to the triple points in the ground-state phase diagram. The infinite-range pure Blume-Capel model ($h_0 = 0$) gives the true behavior of the model in finite dimensions. Also, numerical studies of the Ghatak-Sherrington model in three dimensions

have reported first-order inverse freezing transition [15,16]. We expect our result of the appearance of IT near the triple point of the ground state will hold in finite dimensions for the RFBCM as well.

The absence of IT for symmetric distribution has also been reported for continuous-spin models with random fields like the random-field XY model [45,46]. We expect that the asymmetry in the distribution should induce reentrance in the case of random-field models with continuous spin as well.

For the RFIM it was conjectured that if the phase diagram has a TCP for the symmetric distribution, it will change to a critical end point for any infinitesimal asymmetry [32,34]. The presence of the critical end point implies that the λ -line is still present in the phase diagram. In contrast, for the asymmetric BD defined via Eq. (2), we find that the λ -line and the TCP both disappear completely and there is an OCP instead of a TCP in the phase diagrams.

We also studied the asymmetric Gaussian random-field distribution. The \tilde{f} of the asymmetric Gaussian RFIM is the same as that of the symmetric Gaussian RFIM in an external field of strength equal to the bias in the distribution. Since a symmetric Gaussian RFIM in an external field has finite m at all T that gradually goes to 0 without a phase transition, an asymmetric Gaussian RFIM also has no phase transition. Another interesting distribution is the double-peaked asymmetric Gaussian distribution. This we expect will have phase diagrams similar to those of the asymmetric BD as long as the variance of the distribution is not large.

-
- [1] A. Lindsay Greer, *Nature (London)* **404**, 134 (2000).
 [2] N. Schupper and N. M. Shnerb, *Phys. Rev. E* **72**, 046107 (2005).
 [3] Y. Nahas, S. Prokhorenko, J. Fischer, B. Xu, C. Carrétéro, S. Prosandeev, M. Bibes, S. Fusil, B. Dkhil, V. Garcia, V. Garcia, and L. Bellaïche, *Nature (London)* **577**, 47 (2020).
 [4] O. Portmann, A. Vaterlaus, and D. Pescia, *Nature (London)* **422**, 701 (2003).
 [5] N. Saratz, A. Lichtenberger, O. Portmann, U. Ramsperger, A. Vindigni, and D. Pescia, *Phys. Rev. Lett.* **104**, 077203 (2010).
 [6] N. Saratz, U. Ramsperger, A. Vindigni, and D. Pescia, *Phys. Rev. B* **82**, 184416 (2010).
 [7] J. Brooke, D. Bitko, T. F. Rodenbaum, and G. Aeppli, *Science* **284**, 779 (1999).
 [8] S. Rastogi, M. Newman, and A. Keller, *J. Polym. Sci. B* **31**, 125 (1993).
 [9] S. Rastogi, G. W. H. Höhne, and A. Keller, *Macromolecules* **32**, 8897 (1999).
 [10] M. Plazenet, C. Floare, M. R. Johnson, R. Schweins, and H. Trommsdorff, *J. Chem. Phys.* **121**, 5031 (2004).
 [11] R. Angelini, G. Ruocco, and S. De Panfilis, *Phys. Rev. E* **78**, 020502(R) (2008).
 [12] N. Avraham, B. Khaykovich, Y. Myasoedov, M. Rappaport, H. Shtrikman, D. E. Feldman, T. Tamegai, P. H. Kes, M. Li, M. Konczykowski, K. van der Beek, and E. Zeldov, *Nature (London)* **411**, 451 (2001).
 [13] M. Sellitto and J. Kurchan, *Phys. Rev. Lett.* **95**, 236001 (2005).
 [14] N. Schupper and N. M. Shnerb, *Phys. Rev. Lett.* **93**, 037202 (2004).
 [15] M. Paoluzzi, L. Leuzzi, and A. Crisanti, *Phys. Rev. Lett.* **104**, 120602 (2010).
 [16] L. Leuzzi, M. Paoluzzi, and A. Crisanti, *Phys. Rev. B* **83**, 014107 (2011).
 [17] F. A. da Costa, *Phys. Rev. B* **82**, 052402 (2010).
 [18] A. Crisanti and L. Leuzzi, *Phys. Rev. Lett.* **95**, 087201 (2005).
 [19] L. Leuzzi, *Philos. Mag.* **87**, 543 (2007).
 [20] U. Ferrari and L. Leuzzi, *J. Stat. Mech.* (2011) P12005.
 [21] C. V. Morais, M. J. Lazo, F. M. Zimmer, and S. G. Magalhaes, *Phys. Rev. E* **85**, 031133 (2012).
 [22] C. Morais, M. Lazo, F. Zimmer, and S. Magalhaes, *Physica A (Amsterdam, Neth.)* **392**, 1770 (2013).
 [23] M. Sellitto, *Phys. Rev. B* **73**, 180202(R) (2006).
 [24] C. K. Thomas and H. G. Katzgraber, *Phys. Rev. E* **84**, 040101(R) (2011).
 [25] A. Mendoza-Coto, L. Nicolao, and R. Díaz-Méndez, *Sci. Rep.* **9**, 2020 (2019).
 [26] R. Erichsen and W. K. Theumann, *Phys. Rev. E* **83**, 061126 (2011).
 [27] J. C. Andresen, C. K. Thomas, H. G. Katzgraber, and M. Schechter, *Phys. Rev. Lett.* **111**, 177202 (2013); A. Sera, Y. Kousaka, J. Akimitsu, M. Sera, and K. Inoue, *Phys. Rev. B* **96**, 014419 (2017).
 [28] M. Kaufman and M. Kanner, *Phys. Rev. B* **42**, 2378 (1990).

- [29] P. V. Santos, F. A. da Costa, and J. M. de Araújo, *J. Magn. Magn. Mater.* **451**, 737 (2018).
- [30] S. Mukherjee and Sumedha, *J. Stat. Phys.* **188**, 22 (2022).
- [31] N. G. Fytas and A. Malakis, *Eur. Phys. J. B* **61**, 111 (2008).
- [32] A. Maritan, M. R. Swift, M. Cieplak, M. H. W. Chan, M. W. Cole, and J. R. Banavar, *Phys. Rev. Lett.* **67**, 1821 (1991).
- [33] I. A. Hadjiagapiou, *Physica A (Amsterdam, Neth.)* **389**, 3945 (2010).
- [34] M. R. Swift, A. Maritan, M. Cieplak, and J. R. Banavar, *J. Phys. A: Math. Gen.* **27**, 1525 (1994).
- [35] A. Aharony, *Phys. Rev. B* **18**, 3318 (1978).
- [36] This point is also known as the bicritical end point (BEP) as it is expected that, in a finite uniform magnetic field, two critical lines will meet at this point. For details, see Sumedha and S. Mukherjee, *Phys. Rev. E* **101**, 042125 (2020).
- [37] A. P. Y. Wong and M. H. W. Chan, *Phys. Rev. Lett.* **65**, 2567 (1990).
- [38] G. J. Aubry, F. Bonnet, M. Melich, L. Guyon, P. Spathis, F. Despetis, and P.-E. Wolf, *Phys. Rev. Lett.* **113**, 085301 (2014).
- [39] F. Bonnet, T. Lambert, B. Cross, L. Guyon, F. Despetis, L. Puech, and P. E. Wolf, *Europhys. Lett.* **82**, 56003 (2008).
- [40] E. Kierlik, P. A. Monson, M. L. Rosinberg, L. Sarkisov, and G. Tarjus, *Phys. Rev. Lett.* **87**, 055701 (2001).
- [41] T. Schneider and E. Pytte, *Phys. Rev. B* **15**, 1519 (1977).
- [42] I. D. Lawrie and S. Serbach, in *Theory of Tricritical Points*, edited by C. Domb and J. L. Lebowitz, Vol. 9 (Academic Press, New York, 1984).
- [43] R. Erichsen, Jr., A. A. Lopes, and S. G. Magalhaes, *Phys. Rev. E* **95**, 062113 (2017).
- [44] D. De Martino, S. Bradde, L. Dall'Asta, and M. Marsili, *Europhys. Lett.* **98**, 40004 (2012).
- [45] Sumedha and M. Barma, *J. Phys. A: Math. Theor.* **56**, 095001 (2022).
- [46] C. Lupo, G. Parisi, and Ricci-Tersenghi, *J. Phys. A: Math. Theor.* **54**, 299501 (2021).